Published in final edited form as:
Diabetes. 2008 March ; 57(3): 757–769. doi:10.2337/db07-1441.

Reversal of Streptozotocin-Induced Diabetes in Mice by Cellular Transduction With Recombinant Pancreatic Transcription Factor Pancreatic Duodenal Homeobox-1:

Novel Protein Transduction Domain–Based Therapy

Vijay Koya[1], **Shun Lu**[1], **Yu-Ping Sun**[1], **Daniel L. Purich**[2], **Mark A. Atkinson**[1], **Shi-Wu Li**[1], and **Li-Jun Yang**[1]

[1]Department of Pathology, Immunology, and Laboratory Medicine, University of Florida College of Medicine, Gainesville, Florida

[2]Department of Biochemistry and Molecular Biology, University of Florida College of Medicine, Gainesville, Florida

Abstract

OBJECTIVE—The key pancreatic transcription factor pancreatic duodenal homeobox-1 (Pdx1), known to control development and maintenance of pancreatic β-cells, possesses a protein transduction domain (PTD) that facilitates its entry into cells. We therefore sought to evaluate the capacity of in vivo–administered recombinant Pdx1 (rPdx1) to ameliorate hyperglycemia in mice with streptozotocin-induced diabetes.

RESEARCH DESIGN AND METHODS—Cell entry and transcriptional regulatory properties of rPdx1 protein and its PTD-deletion mutant rPdx1Δ protein, as well as a PTD– green fluorescent protein, were evaluated in vitro. After intraperitoneal rPdx1 injection into mice with streptozotocin-induced diabetes, we assessed its action on blood glucose levels, insulin content, intraperitoneal glucose tolerance test (IPGTT), Pdx1 distribution, pancreatic gene expression, islet cell proliferation, and organ histology.

RESULTS—Restoration of euglycemia in Pdx1-treated diabetic mice was evident by improved IPGTT and glucose-stimulated insulin release. Insulin, glucagon, and Ki67 immunostaining revealed increased islet cell number and proliferation in pancreata of rPdx1-treated mice. Real-time PCR of pancreas and liver demonstrated upregulation of *INS* and *PDX1* genes and other genes relevant to pancreas regeneration. While the time course of β-cell gene expression and serum/tissue insulin levels indicated that both liver- and pancreas-derived insulin contributed to restoration of normoglycemia, near-total pancreatectomy resulted in hyperglycemia, suggesting that β-cell regeneration played the primary role in rPdx1-induced glucose homeostasis.

CONCLUSIONS—rPdx1 treatment of mice with streptozotocin-induced diabetes promotes β-cell regeneration and liver cell reprogramming, leading to restoration of normoglycemia. This novel PTD-based protein therapy offers a promising way to treat patients with diabetes while avoiding potential side effects associated with the use of viral vectors.

Address correspondence and reprint requests to Li-Jun Yang, MD, Department of Pathology, Immunology, and Laboratory Medicine, University of Florida College of Medicine, 1600 SW Archer Rd., P.O. Box 100275, Gainesville, FL 32610-0275. yanglj@pathology.ufl.edu.
V.K. and S.L. contributed equally to this work.

Type 1 diabetes is a metabolic disorder resulting from the autoimmune destruction of pancreatic β-cells. An intense research effort has been directed at identifying a means for restoring β-cell mass as well as glucose-regulated insulin production through islet cell transplantation (1). Though progress has been made, the scarcity of donor islets and the potential need for lifelong immunosuppression will, in theory, greatly limit its potential for widespread application (2). Many alternate strategies have been pursued including vector-mediated delivery of pancreatic transcription factors that allow for conversion of adult cells into insulin-producing cells (IPCs) and for use of cocktails of β-cell growth factors to promote differentiation of embryonic stem cells into tissues capable of producing insulin (3). In vivo, regeneration of residual islet β-cells (1) has been noted to occur with a variety of β-cell growth factors including glucagon-like peptide-1 (4,5), exendin-4 (6, 7), and the islet neogenesis–associated protein (INGAP) (8). These outcomes appear linked to an increased biosynthesis of the pancreatic duodenal homeobox-1 (Pdx1) transcription factor (4,5,7,9,10). Pdx1 is widely regarded as a master transcriptional regulator of the pancreas and is critical for development (11-13), regeneration (10, 14), and maintenance of β-cell function (14,15). Liver stem cells (16) and adult hepatocytes (17,18) reportedly have been reprogrammed by ectopic overexpression of *PDX1* into IPCs that are also capable of restoring euglycemia in diabetic mice. However, the strategies involving the use of viruses as a means for gene delivery in these studies raise safety concerns.

An alternative delivery strategy has recently been identified wherein short, highly basic peptide sequences called protein transduction domains (PTD) act as molecular passports for facile penetration of cellular membranes by proteins (19). Indeed, studies seeking to understand the cell internalization of antennapedia-like homeodomain peptides, a form of PTD, support the view that transcription factors can be transferred from cell to cell, possibly with direct paracrine activity (20, 21). The likely mechanism of cell entry by PTD-containing proteins relies on strong electrostatic interactions of the cationic PTD with phospholipid elements residing in the plasma membrane, followed by macropinocytosis and eventual release into the cytoplasm (19, 22). Once internalized, the protein is then free to exert its biological activity on susceptible targets.

Given its key role in pancreatic development, islet β-cell regeneration, and liver-to-endocrine pancreas transdifferentiation, Pdx1 represents an ideal candidate for protein therapy, especially since its antennapedia-like domain is a PTD, mediating its rapid entry into cells (23-25). Previous in vitro studies involving pancreatic duct and islet cells (23), as well as embryonic stem cells (26), have demonstrated that Pdx1 cell entry induces insulin gene expression and positive autoregulation of Pdx1 gene expression (23, 26). Therefore, the ability of Pdx1 to stimulate insulin gene transcription in vivo renders it a highly attractive approach as a potential treatment for diabetes. In this report, we delivered recombinant rat Pdx1 protein (rPdx1) in vivo in mice with streptozotocin-induced diabetes, monitoring whether rPdx1 would enter into pancreatic or liver progenitor/adult cells, exert transcriptional control on its target genes, and positively autoregulate endogenous *PDX1* gene expression. Herein, we report that, indeed, rPdx1 administration in vivo promotes liver cell transdifferentiation and β-cell regeneration, leading to restoration of normoglycemia in animals with streptozotocin-induced diabetes.

RESEARCH DESIGN AND METHODS

Construction and production of rPdx1, PTD–green fluorescent protein, and mutant Pdx1 fusion proteins

To express recombinant rat Pdx1-His_6 (hereafter designated rPdx1), full-length rat *PDX1* cDNA was amplified by PCR and subcloned using *Nde*I and *Xho*I sites in pET28b (Novagen, Madison, WI). To express PTD–green fluorescent protein (PTD-GFP)-His_6

(hereafter designated PTD-GFP), the *PTD-GFP* plasmid containing the coding sequence for the 11-residue (YGRKKRRQRRR) PTD of HIV-1 TAT positioned at the NH_2-terminus of green fluorescent protein was constructed by PCR and cloned into a pT7/CT-TOPO expression plasmid (Invitrogen, Carlsbad, CA). To prepare the 16-residue PTD-deletion mutant of rPdx1-His_6 (rPdx1-Δmut), we constructed a mutant rat *PDX1* expression plasmid missing PTD residues 188–203 (RHIKIWFQNRRMKWKK) within the rPdx1 homeodomain using PCR amplification with appropriate primers containing sequences before and after the PTD of *PDX1* cDNA. The two PCR products were subsequently ligated to generate the PTD-deletion mutant. After confirmation of the cDNA sequence, the resulting mutant *PDX1* cDNA subcloned into the *Nde*I and *Xho*I sites of pET28b (Novagen). After growth at 37°C to an optical density (OD_{600}) of 0.8, plasmid-containing BL21 (DE3) cells were incubated at room temperature for another 18 h in the presence of 0.5 mmol/l (final concentration) isopropyl β-D-1-thiogalactopyranoside. Bacteria were lysed by pulse sonication in buffer A (20 mmol/l Tris/HCI pH 8.0, 500 mmol/l NaCl, and 0.1% Triton X-100) containing 5 mmol/l imidazole and proteinase inhibitors (Roche Diagnostics, Basel, Switzerland). After centrifugation, the cell-free supernatant was applied to a column of Ni-nitrilotriacetate agarose (Invitrogen) and washed with several volumes of buffer A containing 25 mmol/l imidazole. The protein was eluted by buffer A containing 250 mmol/l imidazole. The purity of the eluted rPdx1, PTD-GFP, and rPdx1-Δmut fusion proteins were characterized by SDS-PAGE/Coomassie Blue staining following dialysis against PBS.

Preparation of pNeuroD-GFP and mouse Pdx1 lentiviral vectors

We constructed, produced, and titered lentiviral vectors (LV) containing the mouse PDX1 cDNA as previously described (27). An LV containing 950 bp (−940 to 10) of human *NeuroD/Beta2* promoter (28) cloned by PCR and ligated into *GFP* was prepared.

Cell entry and immunoblotting

Rat liver epithelial stem cells (WB cells) (29,30) at 70% confluence were treated with purified rPdx1 or rPdx1-Δmut at a 1-μm concentration for various time points, and the cells were washed three times with PBS, harvested in lysis buffer (150 mmol/l NaCl, 50 mmol/l Tris-HCl, pH 7.5, 500 μmol/l EDTA, 1.0% Triton X-100, and 1% sodium deoxycholate) containing a protease inhibitor cocktail (Roche Diagnostics). For Western blotting (27,31), antibodies against rPdx1 (rabbit serum, 1:1,000 dilution, made in our lab using purified rPdx1 as immunogen), his-tag (1:2000; Invitrogen), or actin (1:2000; DAKO, Carpinteria, CA) were used to detect rPdx1, rPdx1-Δmut, actin, or PTD-GFP fusion protein in cell lysates (50 μg total protein/lane) after SDS/PAGE separation.

Cell transduction and flow cytometric analysis

WB cells (70% confluence) were first transduced by LV-pNeuroD-GFP at a multiplicity of infection of 20 as previously described (27). Transduced WB cells were then incubated in the absence or presence of 1 μm rPdx1 protein. *pNeuroD-GFP*–containing WB cells were transduced with *LV-Pdx1*, which served as a positive control for cell-made Pdx1 protein. Cells were harvested 72 h posttreatment, fixed in 1% formaldehyde for 10 min, washed with 1% BSA in PBS, and resuspended. Cytospin slides were prepared with the treated cells and covered with mounting medium containing DAPI.

Animal studies

BALB/c mice (8–10 weeks-old, University of Florida, pathology mouse colony) were injected with 50 mg/kg body wt streptozotocin (Sigma-Aldrich, St. Louis, MO) for 5 consecutive days to induce diabetes (27,31). Animals with fasting blood glucose levels for two consecutive readings of >300 mg/dl received protein treatment. The diabetic mice were

intraperitoneally injected with either rPdx1 or PTD-GFP protein (0.1 mg · day^{-1} · $mouse^{-1}$) for 10 consecutive days. Fasting blood glucose levels were measured regularly using a glucometer after the mice were fasted for 6 h. The sequential experimental events of the animal studies are summarized in Fig. 3*A*.

Intraperitoneal glucose tolerance test

The normal, rPdx1-, or PTD-GFP–treated mice ($n \geq 4$ for each group) were fasted for 6 h following intraperitoneal injection with glucose (1 mg/g body weight), and blood glucose levels were measured at 5, 15, 30, 60, and 120 min postinjection. Subtotal pancreatectomy (>90%) ($n = 4$) was performed at day 30 posttreatment under general anesthesia. The mice were killed at two time points (days 14 or 40 posttreatment), and organs and blood were collected for evaluation of histology, gene expression, serum, and tissue insulin levels.

Pdx1 protein in vivo kinetics and tissue distribution

Mice were injected intraperitoneally with rPdx1 (0.1 or 1 mg). Blood samples were drawn at 0.25, 0.5, 1, 2, 6, and 24 h. Tissues from normal and rPdx1-treated mice were harvested at 1 or 24 h, fixed in 10% formalin, and embedded in paraffin for Pdx1 immunohistochemistry using rabbit anti-Pdx1 antibody (1:3,000; a gift of Dr. Christopher V. Wright, Vanderbilt University). The levels of rPdx1 in sera were determined by immunoblotting as described above.

RT-PCR

Total RNA was prepared from mouse tissues of the pancreas and liver using TRIZOL reagent and cDNA synthesized using Superscript II reverse transcriptase (Invitrogen) with random hexamer primers. Liver gene expression was determined by RT-PCR as previously described (31). The forward and reverse PCR primers were designed to be intron spanning, and their sequences and conditions are listed in Table 1. To eliminate false positives, no reverse transcriptase, positive, or blank controls were included. All data represent at least three measurements from at least four mice.

Quantitative real-time RT-PCR analysis

cDNA from pancreatic and liver tissues was subjected to three independent PCR reactions. Each reaction was performed in duplicate or triplicate in a Thermocycler Sequence detection system (DNA engine opticon 2; MJ Research, Springfield, MO) using SYBR green (Qiagen, Valencia, CA). Total pancreatic and liver RNA was used as templates for preparing cDNA. Tissues were snap-frozen in liquid nitrogen and RNA was extracted in RNase free tubes using Trizol reagent (Invitrogen). The integrity and stability of the RNAs from both pancreas and liver were confirmed by demonstrating the intact 28s and 18s bands on gel electrophoresis. cDNA was synthesized from 5 μg total RNA using Superscript reverse transcriptase enzyme (Invitrogen) with random hexamer primers according to the manufacturer's protocol. Amplication of the correct product was confirmed by gel electrophoresis. Conditions for real-time PCR were as follows: after initial denaturation at 95°C for 15 min to activate the enzyme, 38 cycles of PCR (denaturation 0.5 min at 94°C, annealing 0.5 min at 61°C [for liver] or 56°C [for pancreas], and elongation 0.5 min at 72°C with a final extension 5 min at 72°C) were carried out. Each gene was tested three times (3–4 mice/group). Relative gene expression in mouse pancreas treated by rPdx-1 and PTD-GFP on day 14 was calculated by $2^{-\Delta\Delta Ct}$ method. We used mouse β-actin as internal control and PTD-GFP treated day-14 pancreas cDNA as calibrator. First, both threshold cycle (C_T) values of target gene from rPdx1-treated day-14 pancreas cDNA ($n = 3$) and PTD-GFP–treated day-14 pancreas cDNA ($n = 4$) were normalized by C_T value of the internal control. Then, the former was subtracted by the latter, namely $\Delta\Delta C_{T\ rPdx1/GFP} = (C_{T,\ Target} -$

$C_{T,\ Actin})_{rPdx1} - (C_{T,\ Target} - C_{T,\ Actin})_{GFP}$. Similarly, $\Delta\Delta C_T$ between rPdx1-treated day-14 liver cDNA ($n = 3$) and rPDX1-treated day-40 liver cDNA ($n = 4$, calibrator) was also calculated by $\Delta\Delta C_{T\ day\ 14/day\ 40} = (C_{T,\ Target} - C_{T,\ Actin})_{day\ 14} - (C_{T,\ Target} - C_{T,\ Actin})_{day\ 40}$. The value of $2^{-\Delta\Delta CT}$, the fold change of gene expression, was plotted into the figure. The primers were designed in accordance to the real-time PCR conditions, and the sequences are listed in Table 2.

Immunohistochemistry and immunofluorescence

Paraffin blocks containing the pancreas and liver were obtained from at least 5 mice/group. Antigen retrieval from paraffin sections was done in trilogy solution (Cell Marque, Rocklin, CA) at 95°C for 30 min for unmasking nuclear antigens such as Pdx1 and Ki-67. Paraffin sections (5 μm) were incubated with anti-swine insulin (1:1,000), rabbit anti-Pdx1 (1:5,000), rabbit anti-human Ki67 (1:100; Novus Biologicals, Littleton, CO), and goat anti-glucagon (1:200) antibodies, followed by incubation with anti-mouse or rabbit IgG (1:5,000) conjugated with HRP and detection with DAB substrate kit (Vector Laboratories, Burlingame, CA) as previously described (31). For double immunofluorescence, tissue sections were incubated with anti-swine insulin (1:200) and goat anti-glucagon (1:150; Santa Cruz Biotechnology, Santa Cruz, CA) primary antibody overnight at 4°C, followed by donkey anti–guinea pig IgG conjugated with fluorescein isothiocyanate (1:1,000; RDI Research Diagnostics, Concord, MA) and donkey anti-goat IgG with Alexa flour 594 flourochrome (1:500; Invitrogen). For Ki67/insulin sequential immunostaining, the paraffin sections from pancreas were first immunostained for Ki67 nuclear antigen and developed in brown color using the HRP/DAB system. After being counterstained with hematoxylin to highlight cell nuclei (blue), the slides were immunostained for insulin using guinea pig anti-porcine insulin (cross-react with mouse insulin) antibody (DAKO) at a dilution of 1:200 for 16 min. Presence of insulin in pancreatic islet β-cells was visualized in red color with the Ventana Ultra View red detection kit (Ventana Medical System, Tucson, AR).

Tissue and serum insulin measurements by enzyme-linked immunosorbent assay

Whole pancreas and liver organs were obtained from at least five mice/group. They were harvested, weighed, and immediately placed in acid-ethanol solution (180 mmol/l HCl in 70% ethanol) on ice with a corresponding tissue volume (1 ml buffer/0.1 g liver or 0.05 g pancreas) in accordance with a previously published procedure, with minor modifications (32). Tissue insulin levels were measured using an ultrasensitive mouse insulin enzyme-linked immunosorbent assay (ELISA) kit (ALPCO, Diagnostics, Salem NH). Absorbance was measured using a BIO-RAD 3550-UV microplate reader, with final results converted to nanograms insulin/milligrams pancreas tissue or nanograms insulin/grams liver. For measurement of serum insulin, both normal and treated mice were first fasted for 6 h, and blood samples were collected at 15-min intervals following intraperitoneal glucose (1 mg/g body wt) stimulation. Serum insulin levels were determined by ELISA.

Statistical analysis

Statistical significance was analyzed using an independent sample *t* test, requiring a *P* value <0.05 for the data to be considered statistically significant.

RESULTS

Generation and characterization of recombinant fusion proteins

We constructed expression plasmids containing rat *PDX1*, rat *PDX1*-Δmut, or *PTD-GFP* cDNA, each also containing an additional nucleotide sequence coding for a His_6 tag for rapid purification using Ni^{2+}-nitrilotriacetate columns. To obtain nearly homogeneous

proteins in sufficient amounts for our in vitro and in vivo animal studies, we first optimized bacterial expression conditions to yield 10 mg highly pure rPdx1 per liter of growth medium. Figure 1*A* shows the structural organization of rPdx1 (*a*), PTD-GFP (*b*), and r*PDX1*-Δmut (*c*) and a Coomassie blue-stained SDS gel for rPdx1, PTD-GFP, and rPdx1-Δmut fusion proteins. These proteins consistently had purity >90–95%, based on densitometry. We also confirmed the identity of rPdx1, rPdx1-Δmut, and PTD-GFP proteins by Western blotting with anti-Pdx1 or anti–histidine-tag antibody.

To confirm that rPdx1 protein possessed the ability to penetrate cells due to antennapedia-like PTD within the homeodomain of Pdx1, WB cells were incubated with rPdx1 or rPdx1-Δmut protein (1 μmol/l) for specified times, after which the cells were washed three times with PBS. Cell lysates were separated by SDS-PAGE and blotted with anti-Pdx1 and anti-actin antibodies. The relative amount of rPdx1 in the cell blots was quantified by densitometry and normalized relative to actin. As shown in Fig. 1*Ba*, rPdx1 protein entry commenced within 5 min. As rPdx1 incorporation proceeded, cellular rPdx1 protein level reached peak values at 1–2 h and began to fall by 6 h. In contrast, rPdx1-Δmut with deletion of the 16aa antennapedia-like PTD failed to enter the cells, even though the cell culture medium still contained high levels of rPdx1-Δmut protein (Fig. 1*Bb*).

Since this assay cannot distinguish genuine rPdx1 protein entry versus nonspecific binding to cell membrane surface, we determined whether internalized rPdx1 protein was biologically active. To test the transcriptional function of the rPdx1 protein, WB cells were first transduced with lentivirus-containing pNeuroD-GFP reporter gene, a direct downstream target gene of the Pdx1. The cells were then incubated in the presence or absence of rPdx1 (1 μmol/l) for 72 h. These cells were harvested for flow cytometry to evaluate the rPdx1-mediated NeuroD gene activity by determining the percentage of WB cells expressing pNeuroD-GFP. To compare the efficiency of externally administered rPdx1 vs. endogenous Pdx1, pNeuroD-GFP– containing WB cells were either transduced with LV-Pdx1 (serving as a positive control for endogenous Pdx1) or treated with rPdx1 protein for 72 h, and pNeuroD-GFP–expressing WB cells were determined by both fluorescence microscopy (Fig. 1*Ca*) and flow cytometry (Fig. 1*Cb*). A comparable transcription efficacy for LV-Pdx1–treated cells (21%) and rPdx1 protein–treated cells (19%) after 72 was observed. Both treatments showed statistically significant differences when compared with control cells containing pNeuroD-GFP vector only. These results clearly demonstrated that rPdx1 rapidly entered cells and efficiently activated its downstream *NeuroD* target gene. These findings also confirm that rPdx1 protein has the same or comparable transcriptional activity as endogenous Pdx1 protein produced by means of LV-Pdx1 transgene expression.

In vivo kinetics and tissue distribution

While the antennapedia-like PTD allows in vitro–administered rPdx1 to enter cells, the in vivo tissue distribution and kinetics of rPdx1 were unknown. To examine rPdx1 distribution and kinetics, *BALB/c* mice were intraperitoneally injected with 0.1 or 1 mg rPdx1 protein, blood samples were collected at various times, and rPdx1 was detected in sera by anti-Pdx1 immunoblotting. The rPdx1 became evident in sera as early as 1 h postinjection, reaching peak values at 2 h and then markedly falling by 6 h. No rPdx1 protein was detectable in the 24-h serum samples (Fig. 2*A*). Major organs were harvested at 1 or 24 h after intraperitoneal injection and probed with anti-Pdx1 antibody. As shown in the representative images of liver, pancreas, and kidney tissues (Fig. 2*B*), the rPdx1 was concentrated mainly in the nuclei of hepatocytes, and the greatest intensity of Pdx1-positive cells was found nearest the hepatic terminal veins. This distribution pattern is consistent with the predicted pathway for rapidly internalized rPdx1 via the portal vein system. The rPdx1 was also detected in peripheral acinar cells of the pancreas, possibly as a result of direct uptake or through local circulation along pancreatic terminal capillaries. In kidneys, rPdx1 was mostly concentrated

in brush borders of proximal tubular cells. Little protein was seen in the cytoplasm and none in the nuclei. At 24 h postinjection, only faint rPdx1 protein was focally detected in liver, pancreas, and kidney tissue sections. A low level of rPdx1 was also detected in the tissues of the spleen, heart, lung, and brain at 1 h postinjection, but it became undetectable at 24 h postinjection (data not shown). Similar findings were also noted in mice treated with 1 mg rPdx1 protein. Control mice showed no detectable rPdx1 protein in any tissue section except for pancreatic islet β-cells. On the basis of these findings, we chose the 0.1-mg rPdx1 at 24 h intervals as our in vivo condition for assessing in vivo effects of rPdx1 on mice with streptozotocin-induced diabetes.

In vivo effects of rPdx1 on blood glucose levels in diabetic mice

With this, we developed an experimental timeline for rPdx1 protein administration (Fig. 3*A*) in mice with streptozotocin-induced diabetes (27, 31). Diabetic *BALB/c* mice (body weights ~ 20 g) were intraperitoneally administered with 0.1 mg rPdx1 or nontherapeutic PTD-GFP protein (negative control) over 10 consecutive days. Fasting blood glucose levels were monitored as indicated. Mice receiving rPdx1 injections achieved near normoglycemia within 2 weeks of first injection (Fig. 3*B*); however, no amelioration of hyperglycemia was observed in control mice receiving the PTD-GFP.

At days 14 and 40 postinjection, intraperitoneal glucose tolerance test (IPGTT) (Fig. 3*C*) showed that the mice receiving rPdx1 injection, in contrast to those diabetic mice receiving PTD-GFP, exhibited a much improved, nearly normal IPGTT curve. To further assess the ability of glucose-stimulated insulin release in the rPdx1-treated diabetic mice, healthy normal and treated mice were challenged at days 14 and 40 post-rPdx1 or –PTD-GFP injection with intraperitoneal bolus of glucose. Sera collected from normal, rPdx1-treated, or PTD-GFP–treated mice at 15 min postglucose injection were assayed for insulin and glucose (Fig. 3*D*). Serum insulin levels in rPdx1-treated mice were 6.9 times higher at day 14 and 11.3 times higher at day 40 than those in the PTD-GFP–treated group (Fig. 3*E*), indicating a significant improvement in the ability of the rPdx1-treated mice to handle glucose challenge. Overall, the serum insulin levels were inversely related to the blood glucose levels on days 14 and 40 postinjection in mice treated with rPdx1 or PTD-GFP protein. Although near euglycemia was achieved at day 40 in rPdx1-treated mice, the released insulin (2.6 μg/l) following 15 min of glucose stimulation was still much lower than that in normal nondiabetic mice (5.7 μg/l), suggesting either functional immaturity of newly formed islet β-cells or suboptimal β-cell mass in the pancreas or IPCs in nonpancreatic tissues for glucose homeostasis.

Pdx1 treatment promoting endogenous β-cell regeneration

To explore whether rPdx1-mediated normoglycemia resulted from islet β-cell regeneration, rPdx1-treated mice were subjected to subtotal (>90%) pancreatectomy at day 30 ($n = 4$) postinjection. Blood glucose levels rose sharply following subtotal pancreatectomy (Fig. 3*B*), indicating that pancreatic cells (presumably the islet β-cells) played a dominant role in restoring normoglycemia at 30 days post–rPdx1 injection. To further determine the role of the pancreas at earlier stages of blood glucose normalization, subtotal pancreatectomy was performed at day 12 postinjection in rPdx1-treated mice ($n = 4$) and resulted in elevated blood glucose levels: from an average of 170 to 350 mg/dl within 48 h postoperation (data not shown). These results raise the distinct possibility that in vivo delivery of rPdx1 promoted endogenous β-cell regeneration.

Immunohistochemical examination confirmed vigorous islet β-cell regeneration, with larger and more abundant islets evident in rPdx1-treated mouse pancreata, in contrast to rare and scattered small islets in PTD-GFP–treated mice (Fig. 4*A*). Additionally, individual scattered

insulin-positive cells were also noted within pancreatic acinar cells (data not shown). Such findings indicate that when administered in vivo in multiple doses, rPdx1 appears to promote endogenous β-cell regeneration via an as yet undefined molecular/cellular mechanism. To further characterize the regenerated islets, we conducted double immunofluorescence studies with anti-glucagon and anti-insulin antibodies. Significantly, we noted a change in the α-cell–to–β-cell ratio and distribution patterns (Fig. 4*B*) consistent with a dynamic process of islet cell regeneration and maturation. To determine the proliferation rate in the newly regenerated islets following rPdx1 treatment, we sequentially performed Ki67, followed by insulin immunostaining, on pancreas sections from various groups of animals. As shown in Fig. 4*C*, representative micrographs indicate that Ki67-positive pancreatic islet cells from normal mice were rarely seen (0–1 Ki67 positive cell/islet [Fig. 4*C1*]). Although few proliferating pancreatic islet cells were observed in the PTD-GFP–treated mice, it was difficult to identify normal-sized islets except for scant scattered small islets (Fig. 4*C2*). However, Ki67-positive islet cells were markedly increased in the newly regenerated islets in the pancreata of the rPdx1-treated mice compared with those of control mice. Furthermore, a much higher proliferation index of the islet cells in pancreatic sections was noted in day-14 (Fig. 4*C3*) than day-40 (Fig. 4*C4*) rPdx1-treated mice. Sequential double Ki67/insulin immunostaining (Fig. 4*C5–7a*) showed that both insulin-positive islet β-cells and non–β-cells were proliferating in islets from tissues obtained at days 14 and 40 post–rPdx1 treatment. Interestingly, pancreatic exocrine acinar cells from rPdx1-treated mice also had increased Ki67-positive cells (data not shown).

To determine the molecular events underlying rPdx1-mediated islet β-cell regeneration, we used real-time RT-PCR to examine the expression of key genes relevant to pancreas regeneration. rPdx1 treatment of diabetic mice (Fig. 4*D*) at day 14 resulted in markedly upregulated levels of *INS-I* (21.3 times), *PDX1* (3.8 times), *INGAPrP* (14.5 times), *Reg3γ* (6.8 times), and *PAP* (34.3 times) relative to their corresponding control values (PTD-GFP–treated pancreas). A similar pattern of upregulation of the aforementioned genes was observed at day 40 posttreatment. Interestingly, expression of *PAP*, although upregulated at day 14 when compared with that in PTD-GFP–treated mice, was noticeably reduced at day 40 posttreatment. These results indicate that rPdx1 protein can promote islet β-cell regeneration, possibly by upregulating genes involved in pancreatic cell regeneration.

Pdx1 treatment promoting liver cell transdifferentiation into IPCs

We also assessed whether in vivo intraperiteonal rPdx1 delivery affects the liver by searching for the presence of IPCs in treated mice at days 14 and 40 postinjection. Representative liver images from mice treated with PTD-GFP or rPdx1 at day 14 posttreatment (Fig. 5*A*) indicate that most of the scattered insulin-staining–positive liver cells were distributed along the edges of hepatic terminal veins (H.T.V.), a pattern consistent with rPdx1 tissue distribution in the liver (see Fig. 2*B*). There were scattered individual insulin-positive hepatocytes (arrows) having small bilobed nuclei and dark condensed chromatin, hinting at a more mature cell pattern. No IPCs were observed in the control GFP-treated mouse liver.

We next investigated expression profile of pancreatic genes in rPdx1- and PTD-GFP–treated livers (Fig. 5*B*). As expected, the rPdx1-treated livers at day 14 posttreatment (lane 6) expressed many Pdx1-target pancreatic genes, including *PDX1, INS-I, GLUC, ELAS*, and *IAPP*. Upregulation of other pancreatic endocrine genes (*INS-II, SOM, NeuroD*, and *ISL-I*) and pancreatic exocrine genes (*p48* and *AMY*), was noted in the livers of the rPdx1-treated mice compared with that in the PTD-GFP–treated mice. However, *Ngn3* gene expression was not detectable at either time point. Interestingly, by day 40, *INS-I, GLUC, ELAS*, and *IAPP* gene expression became undetectable, whereas expression of the aforementioned pancreatic genes continued, albeit at reduced levels. To quantitatively compare the changes

of the pancreatic genes in the livers between days 14 and 40, we performed real-time RT-PCR for selected mRNAs including *INS-I, GLUC, PDX1, p48, AMY*, and *ELAS*. As indicated in Fig. 5*C*, a several-fold increase was noted at day 14 vs. day 40 mice post–rPdx1 treatment.

Given the intrinsic ability of rPdx1 protein to penetrate cells indiscriminately, we also examined the tissue specificity of rPdx1's effect on expression of pancreatic *PDX1, INS-I, GLUC*, and *AMY* genes by *RT-PCR*. We found little or no pancreatic gene activation at day 14 post–rPdx1 treatment in kidney, brain, heart, lung, small bowel, or spleen (Fig. 5*D*). These results suggest that rPdx1 selectively promotes liver expression of pancreatic genes and pancreatic β-cell regeneration without detectable evidence of undesired expression in other tissues.

Relationship between pancreas and liver at tissue insulin levels

To determine the relative contribution of pancreas and liver tissue–derived insulin to ameliorating blood glucose levels following rPdx1 treatment, pancreas and liver tissue insulin content of both normal and treated mice was measured at day 14 or 40 by ELISA. Pancreatic insulin content in rPdx1-treated diabetic mice at days 14 and 40 postinjection was ~44 and 68%, respectively, of the normal pancreatic levels (Fig. 6*A*). These levels were also 6.7 times higher at day 14 ($P < 0.01$, Student's t test) and 15.8 times higher at day 40 ($P < 0.001$) posttreatment compared with those in the PTD-GFP–treated diabetic mice.

There is a marked increase (~16 times) in the liver tissue insulin content at day 14 posttreatment in the rPdx1-treated mice over that of the PTD-GFP–treated mice ($P < 0.001$) and nearly a ninefold increase over that of normal liver (Fig. 6*B*). Interestingly, there was sharply reduced liver insulin content at day 40 post–rPdx1 treatment, although it was still 7.3 times higher than that in PTD-GFP–treated mice ($P < 0.01$) and ~2 times higher than that in normal liver. These findings confirmed that in vivo rPdx1 treatment promoted pancreatic islet β-cell regeneration and transient liver cell transdifferentiation into IPCs, suggesting that liver and pancreas both contributed to achieving glucose homeostasis in a compensatory fashion.

DISCUSSION

Given that absolute and relative insulin deficiencies, respectively, form the basis of type 1 and 2 diabetes, the identification of a means for restoring functional β-cell mass would hold immense promise as a means for curing these disorders. In this study, we made several novel findings: *1*) in vivo administration of recombinant Pdx1 ameliorates hyperglycemia in diabetic mice, *2*) amelioration of hyperglycemia is attended by both pancreatic β-cell regeneration and liver cell transdifferentiation, and *3*) the observed therapeutic effect is likely to require Pdx1 to have an intact protein transduction domain. Our experiments therefore constitute a proof-of-principle demonstration that protein therapy in the form of in vivo Pdx1 delivery to whole animals can be a highly effective therapeutic strategy, one that exploits intrinsic properties of a naturally occurring pancreatic transcription factor and that avoids undesirable effects typically associated with viral vector-mediated gene therapies.

Specifically, our results indicate that in vivo delivery of rPdx1 can promote both β-cell regeneration as well as liver cell transdifferentiation into IPCs. Pdx1-mediated pancreatic islet β-cell regeneration appears to be the dominant effect on glucose homeostasis, since marked hyperglycemia was observed in mice receiving nearly total pancreatectomy. Although the exact cellular and molecular events responsible for rPdx1-mediated β-cell regeneration and liver cell transdifferentiation remain to be defined, we believe that, based on our findings, rPdx1 protein enters the circulation via terminal veins and capillaries and

penetrates cellular membranes to gain nucleus entry into target cells in the liver and pancreas (Fig. 2*B*), resulting in activation of rPdx1-dependent transcription factor cascade. The notion that rPdx1 promotes pancreatic β-cell regeneration is supported by the presence of numerous pancreatic large islets (Fig. 4*A* and *B*), an increasing number of proliferating islet cells (Fig. 4*C*), an ensuing increase in the level of pancreatic tissue insulin (Fig. 6*A*), and the significant upregulation of several key genes related to pancreatic cell regeneration in rPdx1-treated mice (Fig. 4*D*). The fact that rPdx1 vigorously promoted pancreatic islet cell proliferation and regeneration raises intriguing questions about the type of pancreatic cells that are the targets of rPdx1 (e.g., what is the cell origin for the newly regenerated islets?). Possible mechanisms include residual islet cell proliferation, exocrine acinar cell transdifferentiation, and pancreatic ductal/stem cell neogenesis. Presently, our approach limits us from tracking the cells of origin into/within the target tissue, resulting in the newly formed islets.

Several genes (*INGAPrP, Reg-3γ*, and *PAP*) upregulated by rPdx1 treatment are members of the pancreatic regenerating (*Reg*) gene family originally identified in animal models of β-cell regeneration (33). Their gene products play important roles in the maintenance of progenitors in the process of pancreas regeneration (10). Despite variation between individual samples, expression levels of the *Reg* genes determined by RT-PCR correlated well with an earlier study involving conditional expression of *PDX1* in a transgenic mouse model (14).

The observed functional effects of rPdx1 on the liver are consistent with the published results of ectopic expression of *PDX1* gene via adenovirus vectors resulting in liver cell transdifferentiation (17, 32). In our experimental models, liver and pancreas appear to work in a sequential, compensatory manner to ameliorate hyperglycemia and ultimately to restore euglycemia in rPdx1-treated mice. The kinship between the liver and pancreas in controlling glucose homeostasis is also supported by a recent study using liver and pancreas double-injury animal models (34). The early phase of rPdx1-induced hepatic insulin production is supported by an intense expression of the insulin I gene (Fig. 5*B* and *C*) and a nearly 18-fold increase in liver tissue insulin in comparison with that of control liver (Fig. 6*B*). While the precise mechanism underlying the rPdx1-mediated surge in hepatic insulin during early-stage glucose homeostasis remains to be elucidated, possible explanations include the following: *1*) action of hepatic insulin on pancreatic progenitor cells via the insulin signaling pathway to promote β-cell regeneration via IRS2-Akt-Pdx1–mediated signal transduction (35); *2*) insulin-mediated facilitation of β-cell neogenesis, involving amelioration of hyperglycemic toxic effects on residual β-cell regeneration (36); and *3*) rPdx1-mediated hepatic insulin production, resulting in an increased rate of glucose clearance by the liver, perhaps by promoting glucokinase expression and/or by insulin's stimulatory action on glycogen synthase, thereby lowering blood glucose levels (37).

Pdx1 expression has also been reported to be associated with β-cell neogenesis in rodent pancreas injury models (10,14,35,38). Although our studies showed roughly a 2 to 4× increase of *PDX1* gene expression in the pancreas of rPdx1- over PTD-GFP–treated mice, pancreatic β-cell function appears to be exquisitely sensitive to small changes in *PDX1* gene expression levels in both humans and mice (38, 39). The rPdx1 protein can positively regulate *PDX1* gene expression, as evidenced by upregulation of endogenous *PDX1* gene expression in the livers of rPdx1-treated mice. These observations are consistent with the findings of others indicating that Pdx1 binds to its own promoter and positively regulates its own gene expression (40). These results suggest that rPdx1-based protein therapy may not require a large-dose or long-term treatment and, thus, may reduce or eliminate potential dosage-related systemic toxicity.

Although we have shown that rPdx1 effectively reverses hyperglycemia in diabetic mice, there are potential obstacles to clinical translation. One concern is that rPdx1 could be partially degraded by serum proteases. To assess this possibility, further studies on rPdx1 stability in whole blood and plasma would be helpful. Moreover, detailed pharmacokinetic studies are needed to optimize dosages, routes of delivery, and the interval between treatments. The polyclonal anti-Pdx1 antiserum used in this study precludes distinguishing between intact and any partially degraded rPdx1 protein. Significantly, the ability of rPdx1 to ameliorate hyperglycemia in diabetic mice, along with its nuclear localization in liver and pancreatic acinar cells (Fig. 2*B*), indicates in vivo availability of a sufficient amount of intact rPdx1 protein or biologically active degradation products capable of translocation into cells. Another concern is the potential toxicity of rPdx1 to off-target organs via its PTD, since the rPdx1 protein has the potential to enter almost any tissue or cell type. We can, however, exclude the activation of rPdx1 target genes in tissues other than liver and pancreas at day 14 posttreatment. Moreover, the animals appeared normal, without evidence of weight loss or abnormal organ morphology. In fact, the diabetic mice treated with rPdx1 gained body weight, showed an improved IPGTT, and exhibited markedly reduced blood glucose levels. Nonetheless, a full toxicity profile of rPdx1, especially at earlier time points, is required to address this question. These studies are beyond the scope of the present manuscript and will be pursued in the future.

Interestingly, the distribution of rPdx1 in the kidney is quite different from that in the liver and pancreas at the early 1-h time point (Fig. 2*B*). Instead of being present in the cell nuclei, rPdx1 was localized near the brush border of the proximal tubular cells (Fig. 2*B3* and 2*B6*). Such a distribution was not observed at 24 h (Fig. 2*B9*). As the rPdx1 protein rapidly enters the bloodstream (Fig. 2*A*) after intraperitoneal injection, it may be filtered through glomerular capillaries into the urinary spaces via the fenestrated capillary endothelial cells and glomerular basement membrane. Alternatively, rPdx1 may gain entry via cells by virtue of its on-board PTD. Once in the urinary spaces, it would not be surprising if the cationic rPdx1 protein interacts electrostatically with polyanions (e.g., sialic acid and phopholipids) present on the apical surface of proximal tubular epithelial cells.

In conclusion, this demonstration that in vivo rPdx1 delivery into diabetic mice rapidly restores euglycemia exploits the intrinsic properties of this key pancreatic transcription factor (e.g., its built-in antennapedia-like PTD, its positive autoregulation, [28, 41], its vital role in pancreatic cell development and regeneration [10, 14], and its role in maintaining pancreatic β-cell function) (14, 15, 42). Indeed, we believe that Pdx1-based protein therapy should allow for a redirection (or reactivation) of pancreatic stem/precursor cell differentiation and transdifferentiation (or reprogramming) from nonpancreatic cells along pancreatic β-cell developmental pathways, a feature that could prove beneficial in treating patients with diabetes.

Acknowledgments

This work is supported in part by National Institutes of Health Grants DK064054 and DK071831 (to L.J. Yang).

We thank Drs. C.V. Wright and W.B. Coleman for providing Pdx1 antibody and WB cell line; L.J. Chang for lentivirus production; D.Q. Tang, S.A. Litherland, and E. Dooley for technical assistance; and J.C. Crawford for critical editorial and scientific inputs.

References

1. Bonner-Weir S, Weir GC. New sources of pancreatic beta-cells. Nat Biotechnol. 2005; 23:857–861. [PubMed: 16003374]

2. Meier JJ, Bhushan A, Butler PC. The potential for stem cell therapy in diabetes. Pediatr Res. 2006; 59:65R–73R.
3. Trucco M. Is facilitating pancreatic beta cell regeneration a valid option for clinical therapy? Cell Transplant. 2006; 15(Suppl. 1):S75–S84. [PubMed: 16826799]
4. Perfetti R, Zhou J, Doyle ME, Egan JM. Glucagon-like peptide-1 induces cell proliferation and pancreatic-duodenum homeobox-1 expression and increases endocrine cell mass in the pancreas of old, glucose-intolerant rats. Endocrinology. 2000; 141:4600–4605. [PubMed: 11108273]
5. Stoffers DA, Kieffer TJ, Hussain MA, Drucker DJ, Bonner-Weir S, Habener JF, Egan JM. Insulinotropic glucagon-like peptide 1 agonists stimulate expression of homeodomain protein IDX-1 and increase islet size in mouse pancreas. Diabetes. 2000; 49:741–748. [PubMed: 10905482]
6. Xu G, Stoffers DA, Habener JF, Bonner-Weir S. Exendin-4 stimulates both β-cell replication and neogenesis, resulting in increased β-cell mass and improved glucose tolerance in diabetic rats. Diabetes. 1999; 48:2270–2276. [PubMed: 10580413]
7. Zhou J, Pineyro MA, Wang X, Doyle ME, Egan JM. Exendin-4 differentiation of a human pancreatic duct cell line into endocrine cells: Involvement of PDX-1 and HNF3beta transcription factors. J Cell Physiol. 2002; 192:304–314. [PubMed: 12124776]
8. Pittenger GL, Taylor-Fishwick DA, Johns RH, Burcus N, Kosuri S, Vinik AI. Intramuscular injection of islet neogenesis-associated protein peptide stimulates pancreatic islet neogenesis in healthy dogs. Pancreas. 2007; 34:103–111. [PubMed: 17198191]
9. Gagliardino JJ, Del Zotto H, Massa L, Flores LE, Borelli MI. Pancreatic duodenal homeobox-1 and islet neogenesis-associated protein: a possible combined marker of activateable pancreatic cell precursors. J Endocrinol. 2003; 177:249–259. [PubMed: 12740013]
10. Sharma A, Zangen DH, Reitz P, Taneja M, Lissauer ME, Miller CP, Weir GC, Habener JF, Bonner-Weir S. The homeodomain protein IDX-1 increases after an early burst of proliferation during pancreatic regeneration. Diabetes. 1999; 48:507–513. [PubMed: 10078550]
11. Holland AM, Hale MA, Kagami H, Hammer RE, MacDonald RJ. Experimental control of pancreatic development and maintenance. Proc Natl Acad Sci U S A. 2002; 99:12236–12241. [PubMed: 12221286]
12. Jonsson J, Carlsson L, Edlund T, Edlund H. Insulin-promoter-factor 1 is required for pancreas development in mice. Nature. 1994; 371:606–609. [PubMed: 7935793]
13. Stoffers DA, Zinkin NT, Stanojevic V, Clarke WL, Habener JF. Pancreatic agenesis attributable to a single nucleotide deletion in the human IPF1 gene coding sequence. Nat Genet. 1997; 15:106–110. [PubMed: 8988180]
14. Holland AM, Gonez LJ, Naselli G, MacDonald RJ, Harrison LC. Conditional expression demonstrates the role of the homeodomain transcription factor Pdx1 in maintenance and regeneration of β-cells in the adult pancreas. Diabetes. 2005; 54:2586–2595. [PubMed: 16123346]
15. Kushner JA, Ye J, Schubert M, Burks DJ, Dow MA, Flint CL, Dutta S, Wright CV, Montminy MR, White MF. Pdx1 restores beta cell function in Irs2 knockout mice. J Clin Invest. 2002; 109:1193–1201. [PubMed: 11994408]
16. Yang LJ. Liver stem cell-derived beta-cell surrogates for treatment of type 1 diabetes. Autoimmun Rev. 2006; 5:409–413. [PubMed: 16890895]
17. Ferber S, Halkin A, Cohen H, Ber I, Einav Y, Goldberg I, Barshack I, Seijffers R, Kopolovic J, Kaiser N, Karasik A. Pancreatic and duodenal homeobox gene 1 induces expression of insulin genes in liver and ameliorates streptozotocin-induced hyperglycemia. Nat Med. 2000; 6:568–572. [PubMed: 10802714]
18. Shternhall-Ron K, Quintana FJ, Perl S, Meivar-Levy I, Barshack I, Cohen IR, Ferber S. Ectopic PDX-1 expression in liver ameliorates type 1 diabetes. J Autoimmun. 2007; 28:134–142. [PubMed: 17383157]
19. Wadia JS, Stan RV, Dowdy SF. Transducible TAT-HA fusogenic peptide enhances escape of TAT-fusion proteins after lipid raft macropinocytosis. Nat Med. 2004; 10:310–315. [PubMed: 14770178]
20. Prochiantz A, Joliot A. Can transcription factors function as cell-cell signalling molecules? Nat Rev Mol Cell Biol. 2003; 4:814–819. [PubMed: 14570063]

21. Joliot A, Prochiantz A. Transduction peptides: from technology to physiology. Nat Cell Biol. 2004; 6:189–196. [PubMed: 15039791]
22. Noguchi H, Matsumoto S. Protein transduction technology: a novel therapeutic perspective. Acta Med Okayama. 2006; 60:1–11. [PubMed: 16508684]
23. Noguchi H, Kaneto H, Weir GC, Bonner-Weir S. PDX-1 protein containing its own antennapedia-like protein transduction domain can transduce pancreatic duct and islet cells. Diabetes. 2003; 52:1732–1737. [PubMed: 12829640]
24. Noguchi H, Matsushita M, Matsumoto S, Lu YF, Matsui H, Bonner-Weir S. Mechanism of PDX-1 protein transduction. Biochem Biophys Res Commun. 2005; 332:68–74. [PubMed: 15896300]
25. Noguchi H, Matsumoto S, Okitsu T, Iwanaga Y, Yonekawa Y, Nagata H, Matsushita M, Wei FY, Matsui H, Minami K, Seino S, Masui Y, Futaki S, Tanaka K. PDX-1 protein is internalized by lipid raft-dependent macropinocytosis. Cell Transplant. 2005; 14:637–645. [PubMed: 16405074]
26. Kwon YD, Oh SK, Kim HS, Ku SY, Kim SH, Choi YM, Moon SY. Cellular manipulation of human embryonic stem cells by TAT-PDX1 protein transduction. Mol Ther. 2005; 12:28–32. [PubMed: 15963917]
27. Tang DQ, Lu S, Sun YP, Rodrigue E, Chou W, Yang C, Chang LJ, Yang LJ. Reprogramming liver-stem WB cells into functional insulin-producing cells by persistent expression of Pdx1- and Pdx1-VP16 mediated by lentiviral vectors. Lab Invest. 2006; 86:83–93. [PubMed: 16294197]
28. Miyachi T, Maruyama H, Kitamura T, Nakamura S, Kawakami H. Structure and regulation of the human NeuroD (BETA2/BHF1) gene. Brain Res Mol Brain Res. 1999; 69:223–231. [PubMed: 10366743]
29. Coleman WB, McCullough KD, Esch GL, Faris RA, Hixson DC, Smith GJ, Grisham JW. Evaluation of the differentiation potential of WB-F344 rat liver epithelial stem-like cells in vivo: differentiation to hepatocytes after transplantation into dipeptidylpeptidase-IV-deficient rat liver. Am J Pathol. 1997; 151:353–359. [PubMed: 9250149]
30. Couchie D, Holic N, Chobert MN, Corlu A, Laperche Y. In vitro differentiation of WB-F344 rat liver epithelial cells into the biliary lineage. Differentiation. 2002; 69:209–215. [PubMed: 11841479]
31. Cao LZ, Tang DQ, Horb ME, Li SW, Yang LJ. High glucose is necessary for complete maturation of pdx-1-vp16–expressing hepatic cells into functional insulin-producing cells. Diabetes. 2004; 53:3168–3178. [PubMed: 15561947]
32. Ber I, Shternhall K, Perl S, Ohanuna Z, Goldberg I, Barshack I, Benvenisti-Zarum L, Meivar-Levy I, Ferber S. Functional, persistent, and extended liver to pancreas transdifferentiation. J Biol Chem. 2003; 278:31950–31957. [PubMed: 12775714]
33. Narushima Y, Unno M, Nakagawara K, Mori M, Miyashita H, Suzuki Y, Noguchi N, Takasawa S, Kumagai T, Yonekura H, Okamoto H. Structure, chromosomal localization and expression of mouse genes encoding type III Reg, RegIII alpha, RegIII beta, RegIII gamma. Gene. 1997; 185:159–168. [PubMed: 9055810]
34. Kim S, Shin JS, Kim HJ, Fisher RC, Lee MJ, Kim CW. Streptozotocin-induced diabetes can be reversed by hepatic oval cell activation through hepatic transdifferentiation and pancreatic islet regeneration. Lab Invest. 2007; 87:702–712. [PubMed: 17483848]
35. Peshavaria M, Larmie BL, Lausier J, Satish B, Habibovic A, Roskens V, Larock K, Everill B, Leahy JL, Jetton TL. Regulation of pancreatic β-cell regeneration in the normoglycemic 60% partial-pancreatectomy mouse. Diabetes. 2006; 55:3289–3298. [PubMed: 17130472]
36. Guz Y, Nasir I, Teitelman G. Regeneration of pancreatic beta cells from intra-islet precursor cells in an experimental model of diabetes. Endocrinology. 2001; 142:4956–4968. [PubMed: 11606464]
37. O'Doherty RM, Lehman DL, Telemaque-Potts S, Newgard CB. Metabolic impact of glucokinase overexpression in liver: lowering of blood glucose in fed rats is accompanied by hyperlipidemia. Diabetes. 1999; 48:2022–2027. [PubMed: 10512368]
38. Waguri M, Yamamoto K, Miyagawa JI, Tochino Y, Yamamori K, Kajimoto Y, Nakajima H, Watada H, Yoshiuchi I, Itoh N, Imagawa A, Namba M, Kuwajima M, Yamasaki Y, Hanafusa T, Matsuzawa Y. Demonstration of two different processes of β-cell regeneration in a new diabetic mouse model induced by selective perfusion of alloxan. Diabetes. 1997; 46:1281–1290. [PubMed: 9231652]

39. Kulkarni RN, Jhala US, Winnay JN, Krajewski S, Montminy M, Kahn CR. PDX-1 haploinsufficiency limits the compensatory islet hyperplasia that occurs in response to insulin resistance. J Clin Invest. 2004; 114:828–836. [PubMed: 15372107]

40. Gerrish K, Cissell MA, Stein R. The role of hepatic nuclear factor 1 alpha and PDX-1 in transcriptional regulation of the pdx-1 gene. J Biol Chem. 2001; 276:47775–47784. [PubMed: 11590182]

41. Marshak S, Benshushan E, Shoshkes M, Havin L, Cerasi E, Melloul D. Functional conservation of regulatory elements in the pdx-1 gene: PDX-1 and hepatocyte nuclear factor 3beta transcription factors mediate beta-cell-specific expression. Mol Cell Biol. 2000; 20:7583–7590. [PubMed: 11003654]

42. Hui H, Perfetti R. Pancreas duodenum homeobox-1 regulates pancreas development during embryogenesis and islet cell function in adulthood. Eur J Endocrinol. 2002; 146:129–141. [PubMed: 11834421]

Glossary

C_T	threshold cycle
IPC	insulin-producing cell
IPGTT	intraperitoneal glucose tolerance test
LV	lentiviral vectors
Pdx1	pancreatic duodenal homeobox-1
PTD	protein transduction domain
PTD-GFP	PTD–green fluorescent protein
rPdx1	recombinant Pdx1

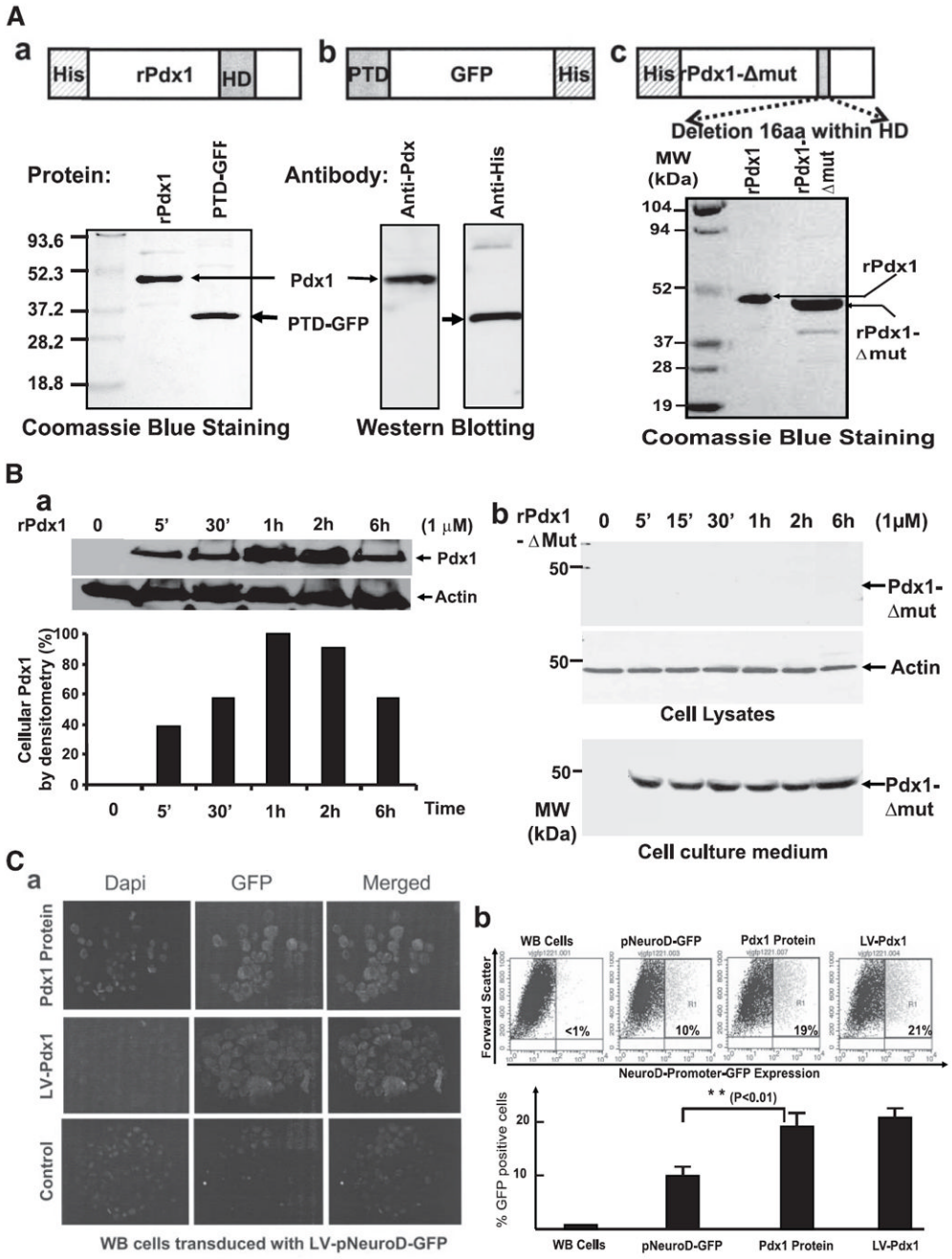

FIG. 1.

Cloning, expression, purification, and characterization of rat Pdx1, PTD-GFP, and rPdx1-Δmut fusion proteins. *A*: Generation of fusion proteins. The top panel represents schematic structures of fusion proteins of rat Pdx1, PTD-GFP, and rPdx1-Δmut. The gray box represents the antennapedia-like PTD in the Pdx1 protein. The cDNAs coding rat Pdx1, mutant Pdx1, or PTD-GFP were cloned into the expression plasmid. Proteins were expressed and purified by an Ni-column. The bottom panel showed purified proteins in a 10% SDS-PAGE gel stained with Coomassie Blue (*left* and *right panels*). The *middle panel* is confirmation of the fusion proteins by Western blotting using anti-Pdx1 antibody (*left lane*) and anti–his-tag antibody (*right lane*). *B*: Time course of cell entry of rPdx1 and

rPdx1-Δmut proteins. WB cells were incubated with rPdx1 or rPdx1-Δmut at a final concentration of 1 μmol/l for indicated times. Proteins were detected by Western blotting with rabbit anti-Pdx1 (1:1,000) or anti-actin (1:5,000) antibodies. The relative amount of cellular rPdx1 protein was quantified by densitometry and the values normalized to actin (*left panel*). The peak reading was defined as 100%, and the remaining values were divided by the highest reading to determine the relative amount of cellular rPdx1 protein. The *right bottom panel* shows rPdx1 protein levels in the culture medium by the end of the treatment. *C*: Functional analysis of rPdx1 protein. WB cells were transduced by the *LV-pNeuroD-GFP* reporter gene. The WB cells expressing *pNeuroD-GFP* reporter gene were visualized and quantified at 72 h posttreatment, with either rPdx1 protein or *LV-Pdx1*, by fluorescence microscopy and flow cytometry. *Left panels* (*a*) show fluorescence images of *pNeuroD-GFP*–expressing cells on cytospin slides. The *right upper panel* (*b*) shows flow dot plots. The *lower panel* is a histogram showing percentage of green fluorescent protein–expressing cells. Data are representative of three independent experiments.

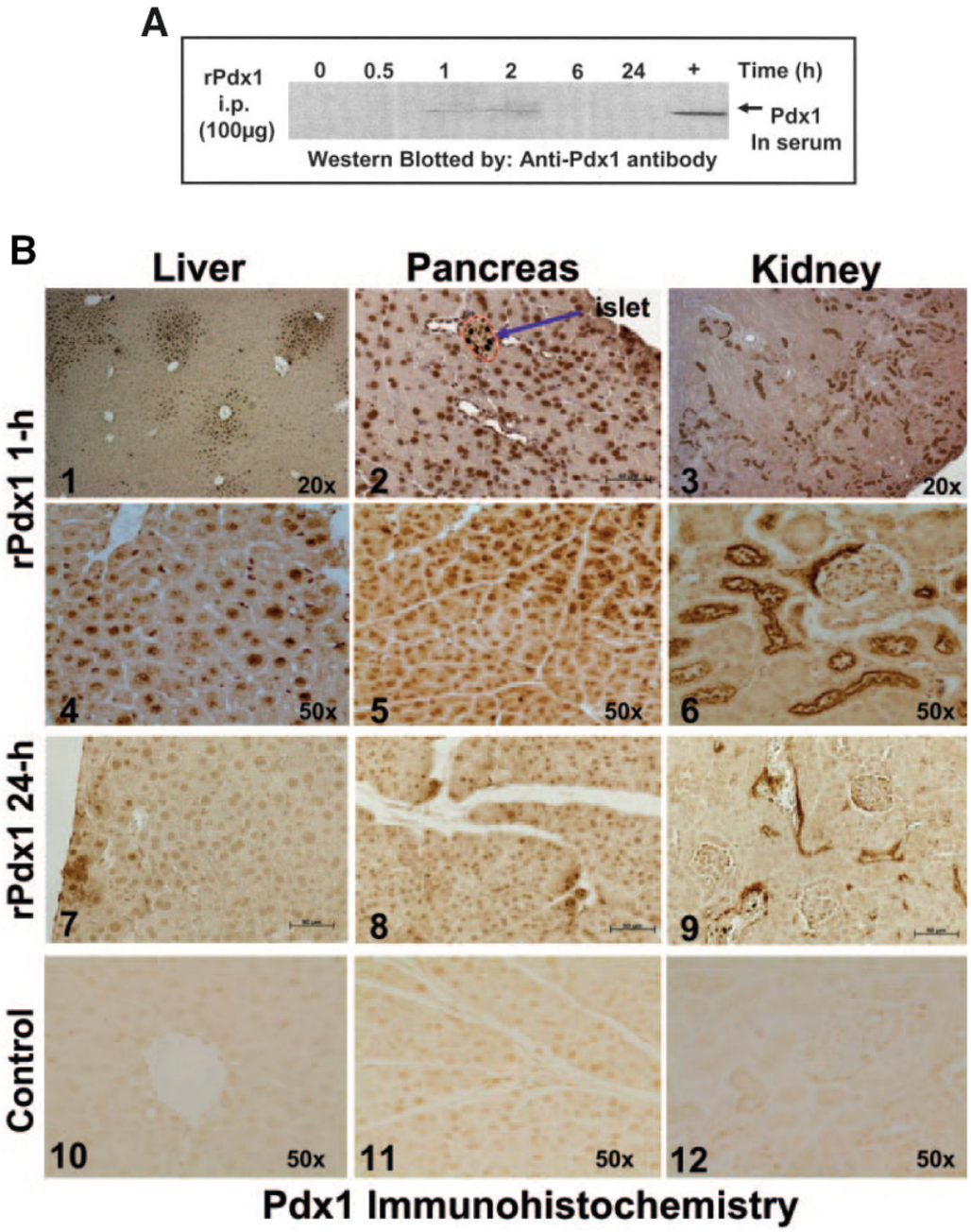

FIG. 2.

In vivo kinetics and tissue distribution of rPdx1 following intraperitoneal injection. *A*: Kinetics of blood rPdx1 levels. Normal BALB/c mice were injected intraperitoneally with rPdx1 protein (0.1 mg/mouse). Blood samples were collected at indicated times, and 20 μl serum/lane was loaded in SDS-PAGE gels. The rPdx1 was detected by Western blotting with anti-Pdx1 antibody. *B*: In vivo tissue distribution of rPdx1. Liver, pancreas, and kidney tissues were harvested at 1 or 24 h after rPdx1 intraperitoneal injection and fixed in 10% formalin. Paraffin sections were immunostained with anti-Pdx1 antibody (1:1,000). Typical distribution patterns of rPdx1 protein in liver (*1, 4*, and *7*), pancreas (*2, 5*, and *8*), and kidney (*3, 6*, and *9*) were visualized by light microscopy at 1 h (*upper two rows*) and 24 h (*third*

row) posttreatment. Pdx1 immunostaining of the liver, pancreas, and kidney tissue sections from normal mice is indicated in the *bottom row* (10-12). The arrow in *B2* indicates a small islet in the pancreas with strong nuclear Pdx1 immunostaining.

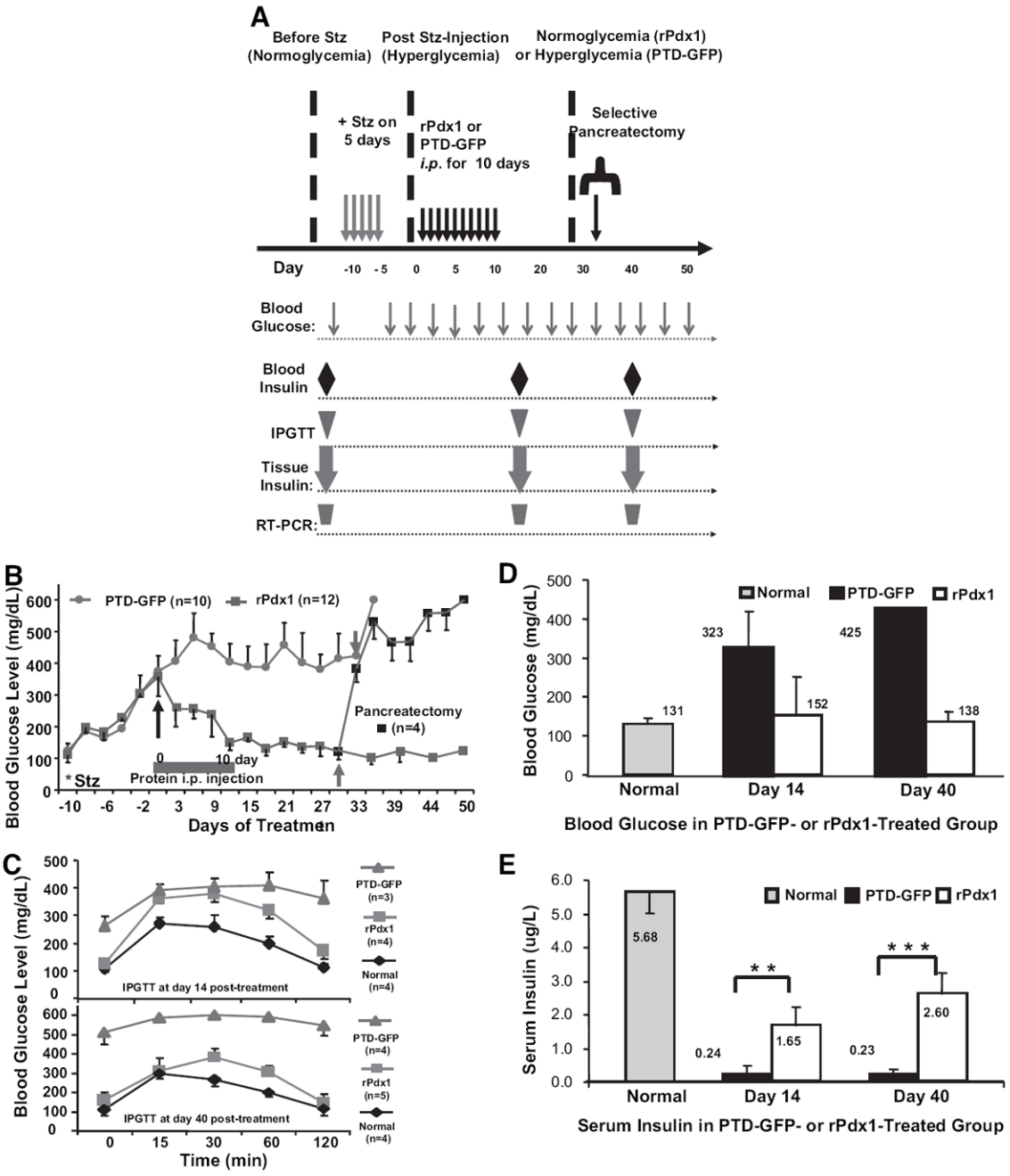

FIG. 3.

A: Experimental timeline. Timing of streptozotocin (Stz) treatment* with rPdx1 or PTD-GFP proteins and selective pancreatectomy are indicated in the *top panel*. The *bottom panel* shows the timing of blood glucose determinations and the measurement of blood insulin levels, IPGTT, measurement of tissue insulin, and the determination of gene expression by RT-PCR (see RESEARCH DESIGN AND METHODS). *B*: In vivo effects of rPdx1 protein on blood glucose levels. Diabetic *BALB/c* mice were treated with daily intraperitoneal injections of 0.1 mg rPdx1 or PTD-GFP for 10 consecutive days (long arrow), and blood glucose levels were determined by glucometer. Nearly total pancreatectomy was performed in selected control and rPdx1-treated mice at day 30 (short arrow). *C*: IPGTT. The IPGTT

was performed as described in RESEARCH DESIGN AND METHODS, and blood glucose was measured at 0, 15, 30, 60, and 120 min in normal, rPdx1-, or PTD-GFP–treated mice. *D*: Blood glucose levels. *E*: Insulin levels following IPGTT. Glucose and insulin levels were measured in rPdx1- and PTD-GFP–treated mice 15 min after IPGTT on days 14 and 40 posttreatment ($n \geq 5$ mice per group). $^{**}P < 0.05$; $^{***}P < 0.001$ (Student's *t* test).

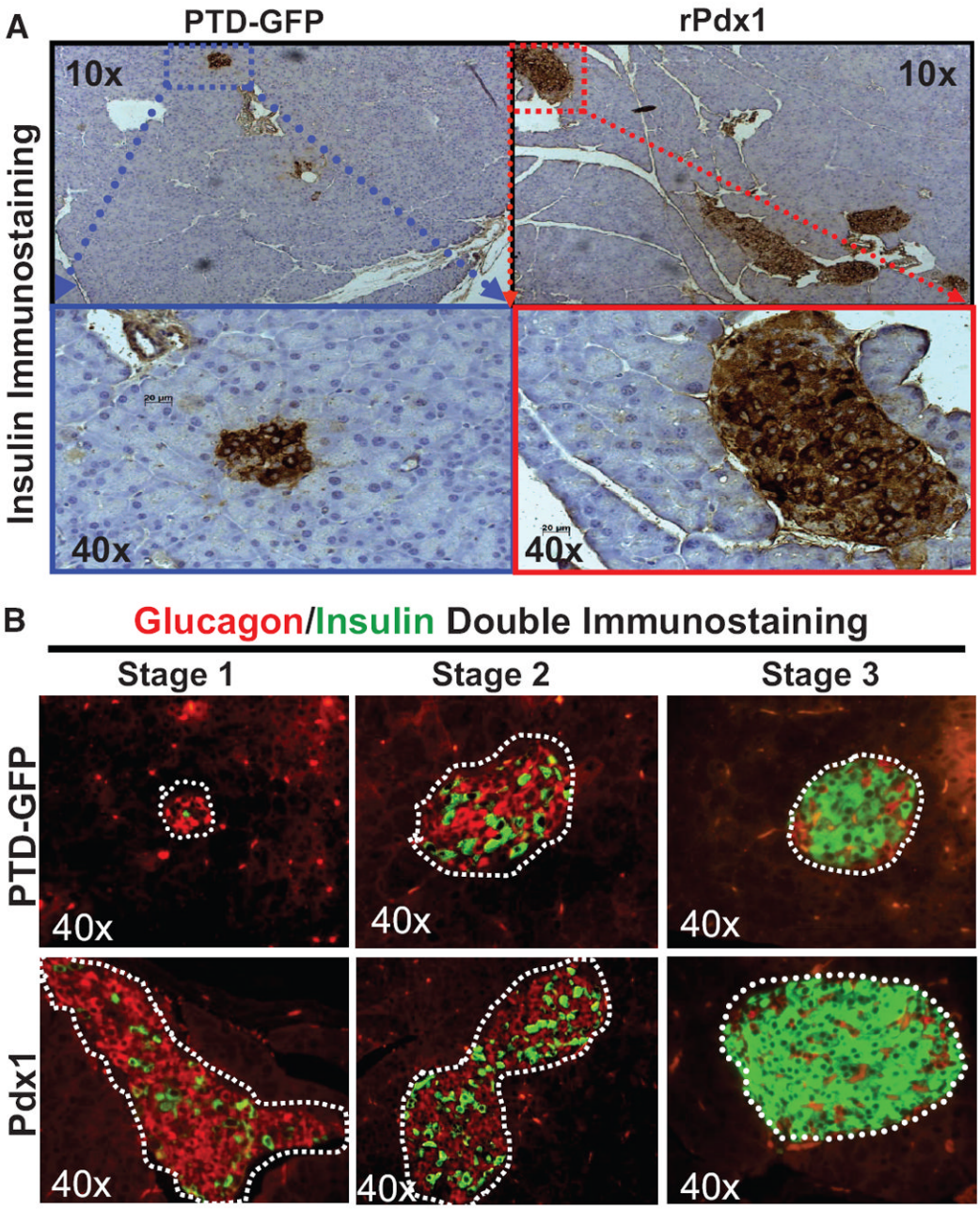

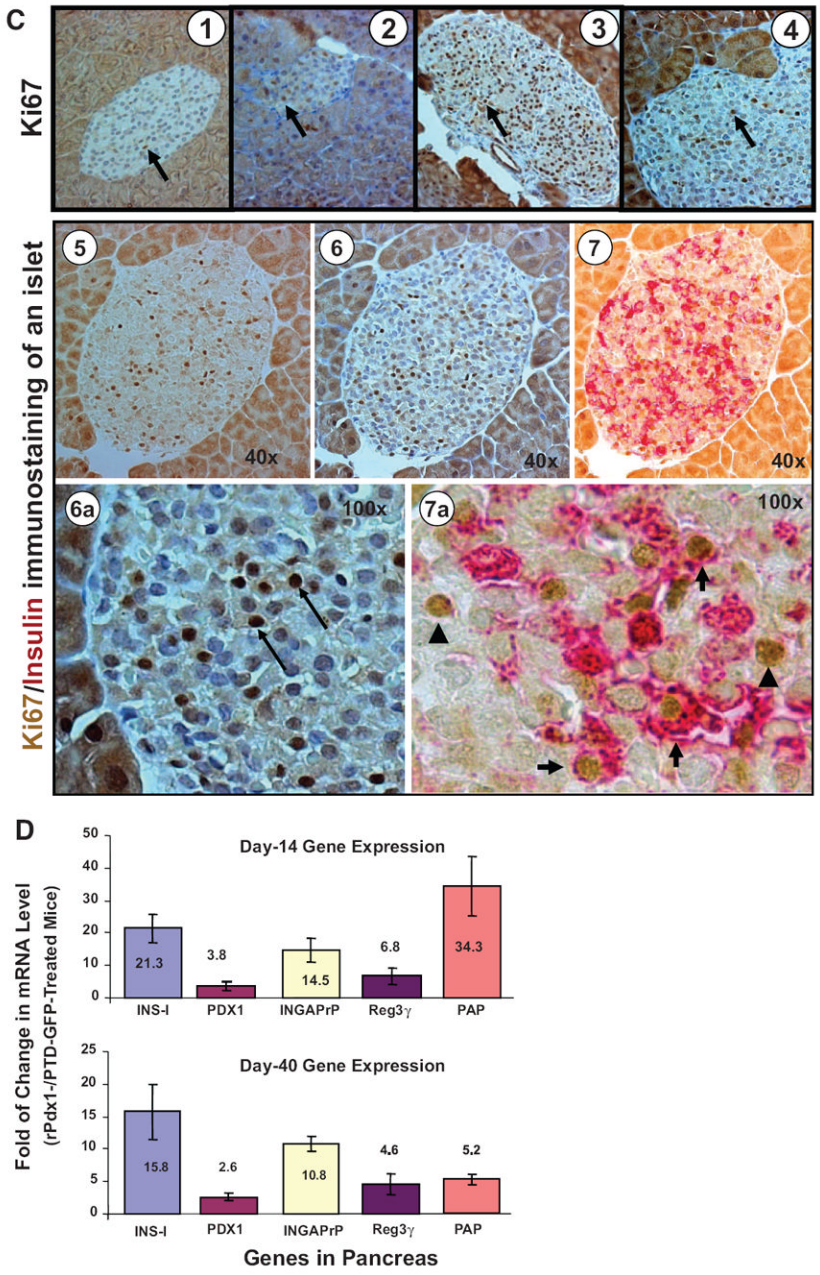

FIG. 4.

Pdx1 protein promotes pancreatic islet cell regeneration. *A*: Insulin immunohistochemistry. Paraffin-embedded pancreas tissues from mice treated with either PTD-GFP (*left*) or rPdx1 (*right*) were sectioned and immunostained with anti-insulin antibody (1:1,000). *B*: Insulin/glucagon double immunostaining of pancreatic tissue. Paraffin sections from PTD-GFP– and rPdx1-treated mouse pancreas tissues were immunostained with both rabbit anti-glucagon/phycoethrin (red) and Guinea pig anti-insulin/FITC (green) and visualized under fluorescence microscopy. Based on the α-cell–to–β-cell ratio and distribution patterns, the pancreatic islets could be arbitrarily divided into three stages: stage 1, α-cell–to–β-cell ratio ~5:1, showing abundant disorganized glucagon-positive α-cells with few scattered β-cells; stage 2, α-cell–to–β-cell ratio 1:1; and stage 3, α-cell–to–β-cell ratio 1:5, showing a

reversed ratio with predominantly insulin-producing β-cells. The architecture of the islets from stage 1 to 3 became more organized, with concurrence of increased numbers of insulin-producing β-cells. *C*: Ki67/insulin immunostaining of pancreatic tissue. Paraffin sections from normal pancreas or pancreas from diabetic mice treated with PTD-GFP or rPdx1 (day 14 or day 40) were first immunostained with anti–nuclear antigen Ki67 antibody (1:100) and then counterstained for nuclear chromatin following antigen retrieval (*Panels 1–4*). *Panels 5–7* show an islet that was first stained for Ki67 (*Panel 5*), counterstained (*Panel 6*), and then stained for insulin (*Panel 7*). *Panels 6a* and *7a* are high-power views of *Panels 6* and *7*. Ki67 nuclear protein was stained in brown (arrows, *Panel 6a*) and cytoplasmic insulin in red. In *panel 7a*, arrowheads indicate non–β cells and arrows β-cells in an islet. *D*: Quantitative RT-PCR analyses. Total RNA from diabetic mouse pancreas (days 14 and 40 post –rPdx1 or –PTD-GFP treatment) was used for real-time PCR analysis of *INS-I, PDX1, INGAPrP, Reg3γ*, and *PAP* gene expression. Expression levels are normalized to actin gene expression.

Data are from ≥3 mice/group. INGAPrP, islet neogenesis-associated protein related protein; PAP, pancreatitis-associated protein; Reg3γ, regenerating islet-derived 3γ.

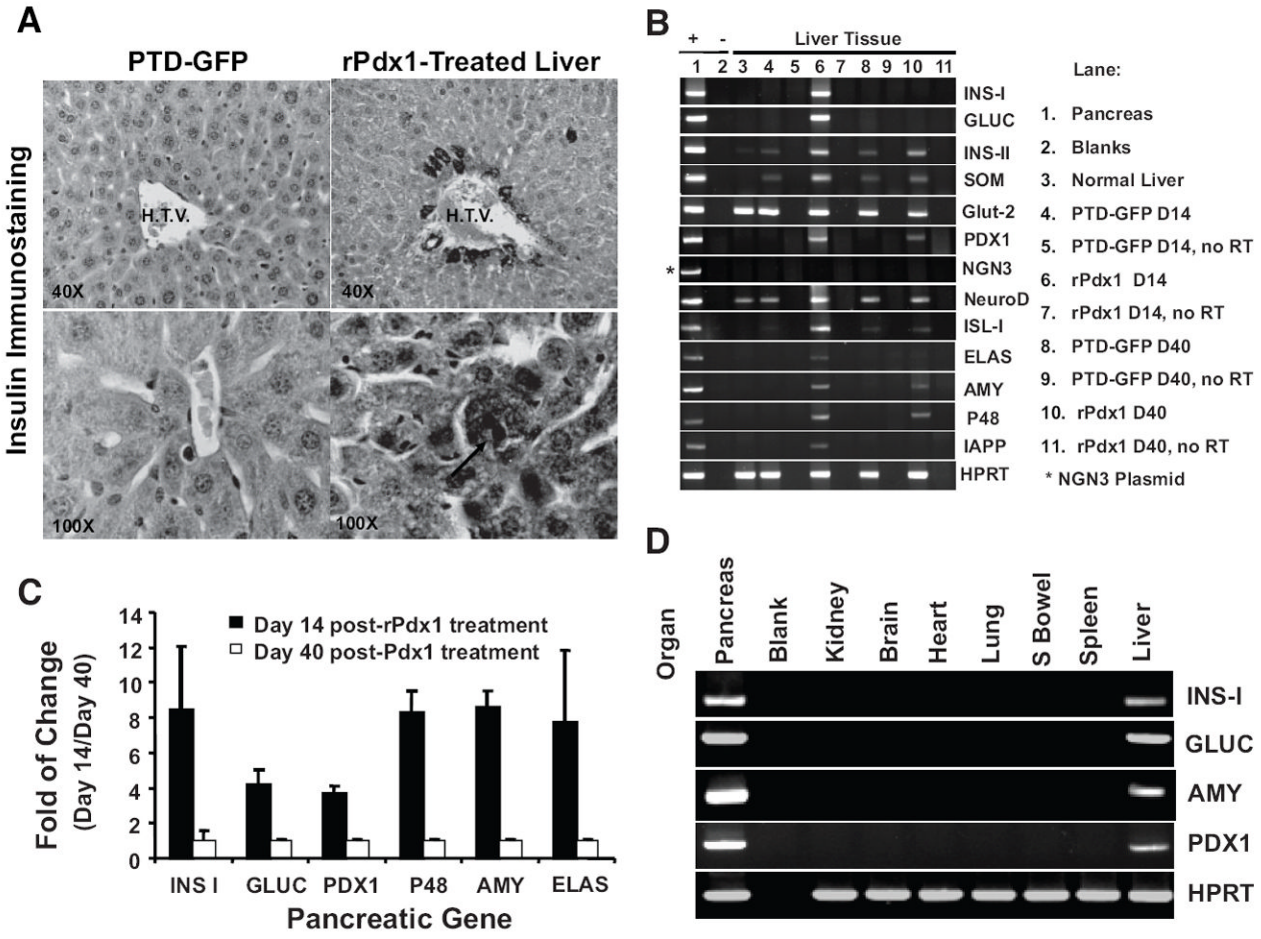

FIG. 5.

Pdx1 protein promotes liver cell transdifferentiation into insulin-producing cells. *A*: Insulin immunohistochemical staining. Paraffin sections from liver were stained with anti-insulin antibody (1:250). Representative images were taken at 40× (*upper panel*) or 100× (*lower panel*) magnification. Insulin-positive cells are seen in the rPdx1-treated mouse liver section at day 14 posttreatment. Arrow, condensed nuclear chromatin of a bilobed-nucleated insulin-expressing liver cell. HTV, hepatic terminal vein. *B*: Expression of pancreatic genes in the liver. RT-PCR amplification of RNA extracted from livers of normal, PTD-GFP–, or rPdx1-treated mice were analyzed by agarose gel electrophoresis. RNA from mouse pancreas was used as a positive control. For Ngn3 RT-PCR analysis, Ngn3 cDNA plasmid (*) was used as positive control because adult pancreas does not express this gene. No RT, no reverse transcription. *C*: Quantitative RT-PCR analyses of pancreatic gene expression in livers. Total RNA from diabetic mouse liver (days 14 and 40 post–rPdx1 treatment) was analyzed by real-time PCR for the expression of five Pdx1 target genes (*INS-I, GLUC, PDX1, p48, AMY, ELAS*). Expression levels are normalized to actin gene expression. Fold changes (D14 over D40) are representative of data from ≥3 mice/group. *D*: Expression of pancreatic genes in other organs. Total RNA from other organs of rPdx1-treated diabetic mice at day 14 posttreatment and expression of four key pancreatic genes (INS-I, GLUC, AMY, and PDX1) were examined by RT-PCR. Data are from ≥3 mice/group and are representative of three independent experiments.

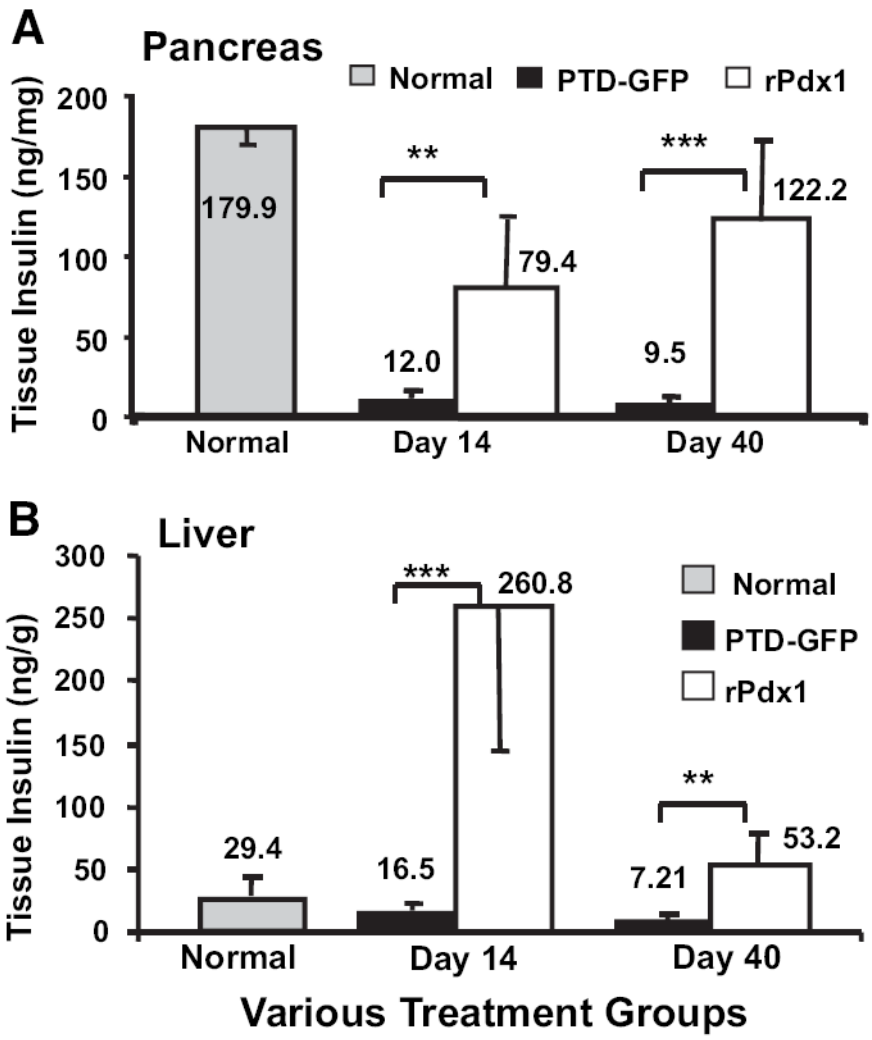

FIG. 6.

Pancreas and liver tissue insulin measurements. *A*: Pancreatic tissue insulin. Normal ($n = 4$) or diabetic mice treated with either PTD-GFP ($n = 4$) or rPdx1 (day 14, $n = 6$; day 40, $n = 5$) intraperitoneally for 10 consecutive days were killed at days 14 or 40 postinjection. The entire liver or pancreas was weighed before extracting tissue insulin to reduce sampling variation. Tissue insulin content in the pancreas is expressed as the amount of insulin (ng/mg) wet weight of pancreatic tissue. $^{**}P < 0.05$; $^{***}P < 0.001$, Student's *t* test. *B*: Liver tissue insulin measurement. Liver tissue insulin was extracted as described above. Insulin content is expressed as the amount of insulin (ng/g) wet weight of liver tissue. At day 14, the liver insulin content was significantly higher in the rPdx1-treated mice ($n = 6$) than in liver from normal ($n = 4$) or PTD-GFP–treated ($n = 5$) mice. $^{**}P < 0.05$; $^{***}P < 0.001$, Student's *t* test.

TABLE 1

Primer name, sequences, size, GenBank accession no., and PCR condition

Genes	Forward primer	Reverse primer	PCR size (bp)	GenBank accession no.	Tm (°C)	Cycle no.
HPRT	CTCGAAGTGTTGGATACAGG	TGGCCTATAGGCTCATAGTG	350	NM_013556	56	40
INS-I	TAGTGACCAGCTATAATCAGAG	CAGTAGTTCTCCAGCTGGTA	372	NM_008386	56	40
INS-II	GCTCTTCCTCTGGGAGTCCCAC	CAGTAGTTCTCCAGCTGGTA	288	NM_008387	56	40
GLUC	TGAAGACCATTTACTTTGTGGCT	TGGTGGCAAGATTGTCCAGAAT	492	NM_008100	57	40
SOM	CTCTGCATCGTCCTGGCTTTG	GGCTCCAGGGCATCATTCTCT	173	NM_009215	56	40
IAPP	TGAACCACTTGAGAGCTACAC	TCACCAGAGCATTTACACATA	282	NM_010491	55	40
Glut-2	CGGTGGGACTTGTGCTGCTGG	GAAGACGCCAGGAATTCCAT	412	NM_031197	56	40
P48	CCCAGAAGGTTATCATCTGCC	CGTACAATATGCACAAAGACG	245	NM_018809	57	40
ELAS	AATGACGGCACCGAGCAGTATGT	CCATCTCCACCAGCGCACAC	344	NM_033612	57	40
AMY	TGGGTGGTGAGGCAATTAAAG	TGGTCCAATCCAGTCATTCTG	371	NM_009669	56	40
PDX1	ACCGCGTCCAGCTCCCTTTC	CCGAGGTCACCGCACAATCT	357	NM_008814	57	40
NeuroD1	CATCAATGGCAACTTCTCTTT	TGAAACTGACGTGCCTCTAAT	257	NM_010894	56	40
ISL-1	AGACCACGATGTGGTGGAGAG	GAAACCACACTCGGATGACTC	296	NM_021459	56	40
NGN3	TGGCACTCAGCAAACAGCGA	AGATGCTTGAGAGCCTCCAC	516	NM_009719	56	40

AMY, amylase 2; *ELAS*, elastase 1; *GLUC*, glucagon; *IAPP*, islet amyloid polypeptide; *ISL-I*, islet-1; *NGN3*, neurogenin 3; *SOM*, somatostatin.

Diabetes. Author manuscript; available in PMC 2012 August 14.

TABLE 2

Real-time PCR primer name, sequences, size, GenBank accession no., and PCR condition

Genes	Forward primer	Reverse primer	PCR size	GenBank accession no.	Tm (°C)	Cycle no.
Actin	ACCACACCTTCTACAATGAGC	GGTACGACCAGAGGCATACA	185	NM_007393	56	38
INS-I	GCCCTTAGTGACCAGCTAT	GGACCACAAAGATGCTGTTT	154	NM_008386.2	56	38
PDX1	ATGAAATCCACCAAAGCTCAC	AGTTCAACATCACTGCCAGCT	190	NM_008814.2	56	38
INGAPrP	GCTCTTATCTCAGGTTCAAGG	AGATACGAGGTGTCCTCCAGG	178	NM_013893.1	56	38
Reg3γ	CATGACCCGACACTGGGCTATG	GCAGACATAGGGTAACTCTAAG	190	NM_011260.1	56	38
PAP	AATACACTTGGATTGGGCTCC	CCTCACATGTCATATCTCTCC	195	NM_011036.1	56	38
GLUC	GCACATTCACCAGCGACTACA	TGACGTTTGGCAATGTTGTTC	109	NM_008100.3	61	38
P48	GAGAGGACAGTCCCGGTAACC	AAAGAGAGTGCCCTGCAAGAG	117	NM_018809.1	61	38
AMY	AAGTGGAATGGCGAGAAGATG	ATGATCCTCCAGCACCATGTC	130	NM_009669.2	61	38
ELAS	ATCACAGGCTGGGGAAGAAC	TTCACAGAGGAGCCCCAGTAA	122	NM_033612.1	61	38

INGAPrP, islet neogenesis associated protein-related protein; *P48*, pancreas specific transcriptional factor-1α.